Shock initiation experiments and reactive flow modeling analysis for pentaerythritol tetranitrate (PETN) high explosive

Carlos Chiquete, Malcolm J. Burns, Eric K. Anderson
Los Alamos National Laboratory
Los Alamos, NM, USA
Scott I. Jackson
Texas A&M University
College Station, TX USA

1 Introduction

Pentaerythritol tetranitrate (PETN) is a commonly used explosive in detonator applications at a variety of pressing densities, motivating its previous experimental characterization [1, 2, 3]. Recently however, engineering applications using the explosive have used a target pressing density of 1.65 g/cm^3, which is not specifically reflected in these now archival data sets. Hence, the detonation performance of PETN (i.e. timing and energy delivery) at this new density was recently investigated [4] using modern diagnostic techniques and test geometries. Given the extremely short reaction zone of PETN, miniaturized rate sticks and a cylinder expansion test [4] (i.e. at $\approx$ 1/8 scale) were fielded in order to generate measurable finite reaction zone effects and therefore constrain the reaction zone structure of detonating PETN. Nevertheless, in spite of the minute scale, continuum-level detonation performance modeling techniques proved effective at representing the recorded performance data [4]. Note that sufficiently accurate theoretical means are still lacking requiring this extensive experimental characterization effort.

Here, we utilize new plate impact experiments to characterize the initiation of PETN at 1.65 g/cm^3 pressing density, complementing the previous performance characterization [4]. The present cut-back style tests use a series of extremely thin explosive samples to fully capture the likewise rapid transition to detonation for a variety of conditions. Our results represent a significant expansion of initiation data for the explosive since similar experiments reported in [5] were only able to capture this for a single impact condition. Additionally, we report on our reactive flow modeling analysis for PETN using the totality of data reported here and in [4]. We also use the initiation rate calibration process to assess the consistency of the plate-impact experiments for all experimental conditions, quantifying the resulting experimental variability with an entirely novel methodology. In contrast to similar modeling efforts reported in [5], the relevant reactive flow model components developed here are directly derived from the available front curvature and metal push measurements and should improve their predictive capability, especially when and where detonation propagation transitions to quasi-steady flow. In the following, we report on new plate-impact-driven initiation tests and then present a description of the attendant modeling effort.

2 Experiments

In order to achieve the small sample thicknesses required to capture the partial reaction profiles for a extremely reactive material such as PETN, the explosive powder was pressed into small Al-1100 cups

Correspondence to: chiquete@lanl.gov

Table 1: (left) Metrology data for pressed PETN. (right) Experimental input conditions, where U_{Proj} is the projectile velocity, u_p is the particle velocity as measured at the first probe location and p_{input} is the impedance-matched and model-derived input pressure. The setup type corresponds to Fig. 1.

Nominal Thickness (mm)	Measured Thickness (mm)	Density (g/cm^3)
0.50	0.543(2)	1.654(3)
0.75	0.662(2)	1.652(3)
1.00	0.905(1)	1.653(3)
1.25	1.241(1)	1.650(2)

Shot No.	Impactor	U_{Proj} (km/s)	u_p (mm/μs)	p_{input} (GPa)	Setup Type
1s-1700	Al 1100	0.816(1)	0.364(3)	3.12	A
1s-1701	Al 1100	0.897(2)	0.409(7)	3.55	A
2s-1132	Kel-F	1.438(3)	0.435(10)	3.74	B
2s-1133	Kel-F	1.516(2)	0.560(35)	4.06	B
2s-1131	Al 1100	1.238(3)	Detonation	5.47	B

(see Fig. 1). This meant that the experiments had to be designed as a cut-back style target where window interface velocities are recorded for variety of HE thicknesses, as opposed to embedded gauge experiments which provide in situ reactive growth measurements. To simplify shock interactions, a cover disc of Al-1100 was also used. The PETN samples were pressed to a series of targeted, nominal heights: 0.50, 0.75, 1.00 and 1.25 mm. The PETN was then pressed into the cups with the specification to maintain a density of 1.65 g/cc while keeping the target thicknesses as close as possible to the nominal values (significant departures did occur as shown in Table 1(left) which presents the metrology data for the samples).

A schematic of the experimental setup is shown in Fig. 1, and highlights the two variants of experimental design. The optical diagnostics used to record the motion of the PETN and Lithium Flouride (LiF) interface in these experiments included both Velocity Interferometer System for Any Reflector (VISAR) and Photon Doppler Velocimetry (PDV). The first two experiments were carried out using setup A. This initial design intended to provide a larger suite of data from each experiment. In these experiments, there were two cups for each sample height. With the final three experiments, a simplified setup was used (setup B) with one sample for each height. This change was made due to the size of the PETN cups resulting in the observation of edge effects in some of the optical measurements of the first 2 experiments using setup A. As such, a single channel of PDV was used in the center of each sample in the three final experiments. The experiments were carried out using both single and two-stage gas

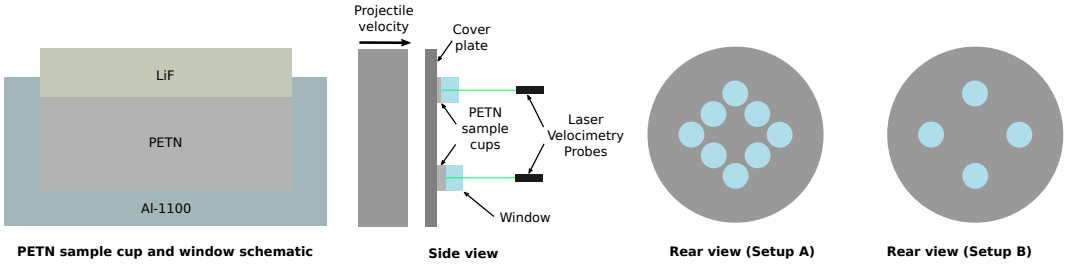

Figure 1: Schematic of the PETN sample in its cup as well as the general experimental setup.

guns and used Al-1100 and polychlorotrifluoroethylene fluoropolymer (or "Kel-F") impactors in order to achieve the desired input pressures. In previous work, Stirpe [2] studied the run to detonation of both 1.6 and 1.72 g/cc pressed PETN using an explosive driver system and streak imaging to determine the detonation coordinates and this was used to approximately infer the initial impact conditions and aid in the initial experimental design. The projectile velocities and particle velocities measured at the first probe location are shown in Table 1(right). The resulting measurements of the window velocity are shown in Fig. 4 (note that tilt-correction was applied to the time-of-arrival data for each experiment). As can be seen, 4 of the 5 experiments resulted in clear evidence of turnover to detonation. Figure 2 presents the common historical methodology to represent the relative sensitivity of explosives, i.e. input

pressure and run distance to detonation or the "Pop-plot". In particular, the present turnover results are compared with analogous data from [2] at 1.6 and 1.72 g/cm^3 pressing densities, lying between the reference trend lines from previous work.

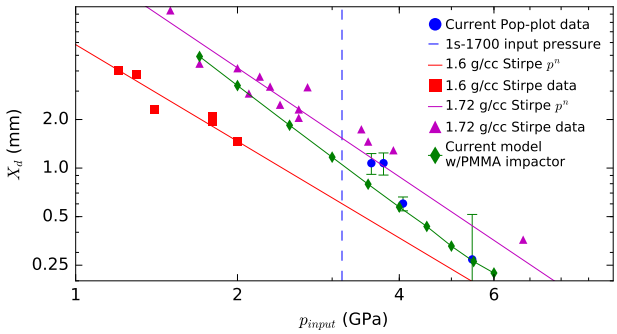

Figure 2: Run distance (X_d) vs input pressure (p_{input}) for 1.6 and 1.72 g/cm^3 PETN from [2] and current results at 1.65 g/cm^3. Shown X_d calculations used a calibrated model obtained here and a poly(methyl methacrylate) (PMMA) impactor (since Stirpe [2] used this in his impactor system).

3 Reactive flow model calibration

Our computational analysis of both the present initiation and performance data for PETN uses a modified Wescott-Stewart-Davis (MWSD) reactive flow model. How it specifically differs with the original definition of the WSD [6] model and our chosen calibration methodology is detailed in the following.

Equations of state: For our modeling purposes, the Davis equation-of-state (EOS) state functions relating the internal energy (e) and pressure (p) for can be stated as $p = p_s + (\Gamma(v)/v)(e - e_s)$, for both the reactants and products phases. For brevity, we omit the specific reference isentrope functions (e_s and p_s) and the Mie-Grüneisen gamma functions but can refer the reader to Ref. [7] for a complete the definition of the Davis forms and parameters. For the reactants, the EOS parameters (see Table 2) are calibrated with reference to the window velocity profiles and arrival times recorded in the initiation experiments, given the lack of direct in situ measurements of the shock response of this material. The calibrated products EOS parameters (see Table 2) are based on the pressure isentrope model obtained in [4] but translated into the Davis form via a curve-fitting process based on the isentrope and CJ state (similar to translation process used in [8]). The resulting cylinder expansion test wall motion is excellently represented using the Davis products model, as shown in Fig. 3(left). The calculation was performed using a multi-physics multi-material hydrocode (see [4, 7, 9] for a fuller description of numerical methodology) and a 15 micron resolution. The pressure isentrope variation is also plotted in the inset of Fig. 3(left).

Reactive rate and closure model definition: The modified reaction rate that we choose to calibrate is

$$\Lambda(\lambda, p, \rho_s) = W k_i (1-\lambda)^c p^y + (1-W) k_g (1-\lambda)^c p^n, W = \frac{1}{2}\left(1 - \tanh\left(50\left[\frac{\rho_s}{\rho_c} - 1\right]\right)\right). \quad (1)$$

The rate depends on the local pressure (p), shock density (ρ_s), reaction progress (λ) and the rate parameters k_i, c, y, k_g, n and ρ_c. Here, we have also modified the EOS closure of the model, from $p - T$ to the $p - \rho$ for reasons of computational efficiency. There are two other terms in the base WSD rate as originally defined, the selected terms shown above are sufficient to adequately represent the available initiation and propagation data. The disjoint activation of the initiation and propagation terms (via the blending function W) allows for a sequential calibration process. As a result, it is possible apply different source data sets and numerical machinery to efficiently calibrate each rate term.

Propagation regime calibration: The rate stick simulations needed to infer the reaction zone (RZ) structure were carried out in an efficient shock-attached two-dimensional framework (see [10]). The detonation RZ structure for our present model is controlled by the c, n and k_g parameters and these were varied in order to produce the front shape comparison between data and calculation in Fig. 3(right). The correspondence is good and again reinforces the fact that the data reported in [4] can be represented by our usual continuum-level reactive flow methodologies, despite the extremely rapid reaction in this material (i.e. completed on a ns timescale). As a result, the front shape calculation in Fig. 3(right) used a resolution of a quarter micron to reasonably resolve the RZ. In the inset of Fig. 3(right), the calculated diameter effect also appears along with the detonation velocity data gathered to this date. Parameters

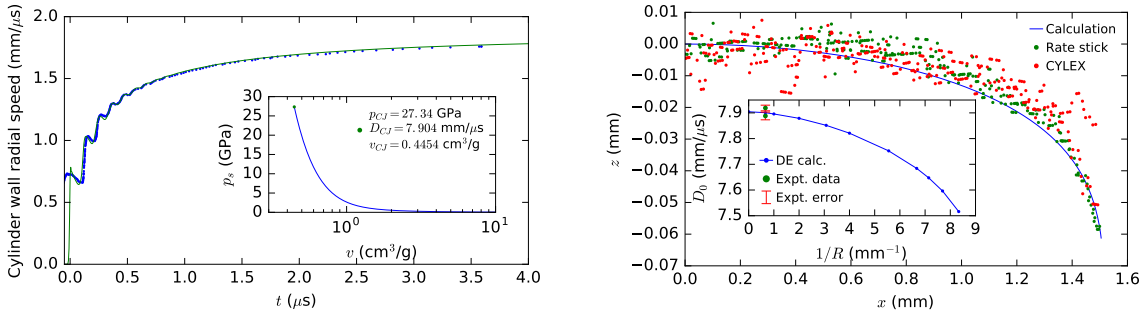

Figure 3: (left) The calculated and experimental outer wall (radial) motion for the 3 mm CYLEX test. Inset gives the pressure isentrope variation and CJ state (right) The calculated and experimental front shape for the 3 mm rate stick test. Inset presents the diameter effect comparison.

for this rate term appear in Table 2.

Shock initiation calibration: To calibrate the initiation rate parameters, k_i, y and ρ_c, calculations were carried out to compare to the window velocity measurements shown in Fig. 4 (bottom). These simulations represent the plate impact experiments where the HE initiation takes place via a one-dimensional planar shock, with materials and models approximating the shot geometries shown in Fig. 1. Simulations were iteratively performed using an adaptive mesh refinement (AMR) enabled multi-material methodology described in [11] and used a finest resolution of 6.25 microns (which appeared sufficient to represent the reactive build-up in the PETN). Standard linear $u_s - u_p$ EOS models were used for the inert materials in the experiments (Al, Kel-F and LiF), each calibrated to existing shock Hugoniot data.

At this point, it is conventional to calibrate all available initiation data sets using a single model parameterization. In this case however, we instead embarked on an exercise in calibrating to each individual profile produced in our experiments, generating as many reaction rate parameterizations which can then be compared for their consistency. This process produced the fitting error matrix plot shown in Fig. 4(top) which plots the error (based on sum of squared differences in window velocity) associated with a calibration performed only on a single trace and the corresponding prediction error associated with that model with every other single trace in our shot compendium. This was meant to quantify the intra-consistency of each experiment and profile given the possibility of initial density variations or other sources of variability. The blue color indicates low error and red indicates large errors (all relative to the calibration fit error of each profile). The main insight revealed in this plot is that when each of the 1s-1700 and 1s-1701 profiles are calibrated individually we obtain models which are significantly less reactive than the high input pressure counterparts (2s-1131, 2s-1132 and 2s-1133) and generate large errors as the turn-over occurs far too late. The reverse is also true though to a lesser extent. Therefore, this modeling analysis shows that there is a disjoint behavior between the lower and higher input pressure tests. Also, in several cases, the thinnest HE width profile (and therefore least reactive) seems to be

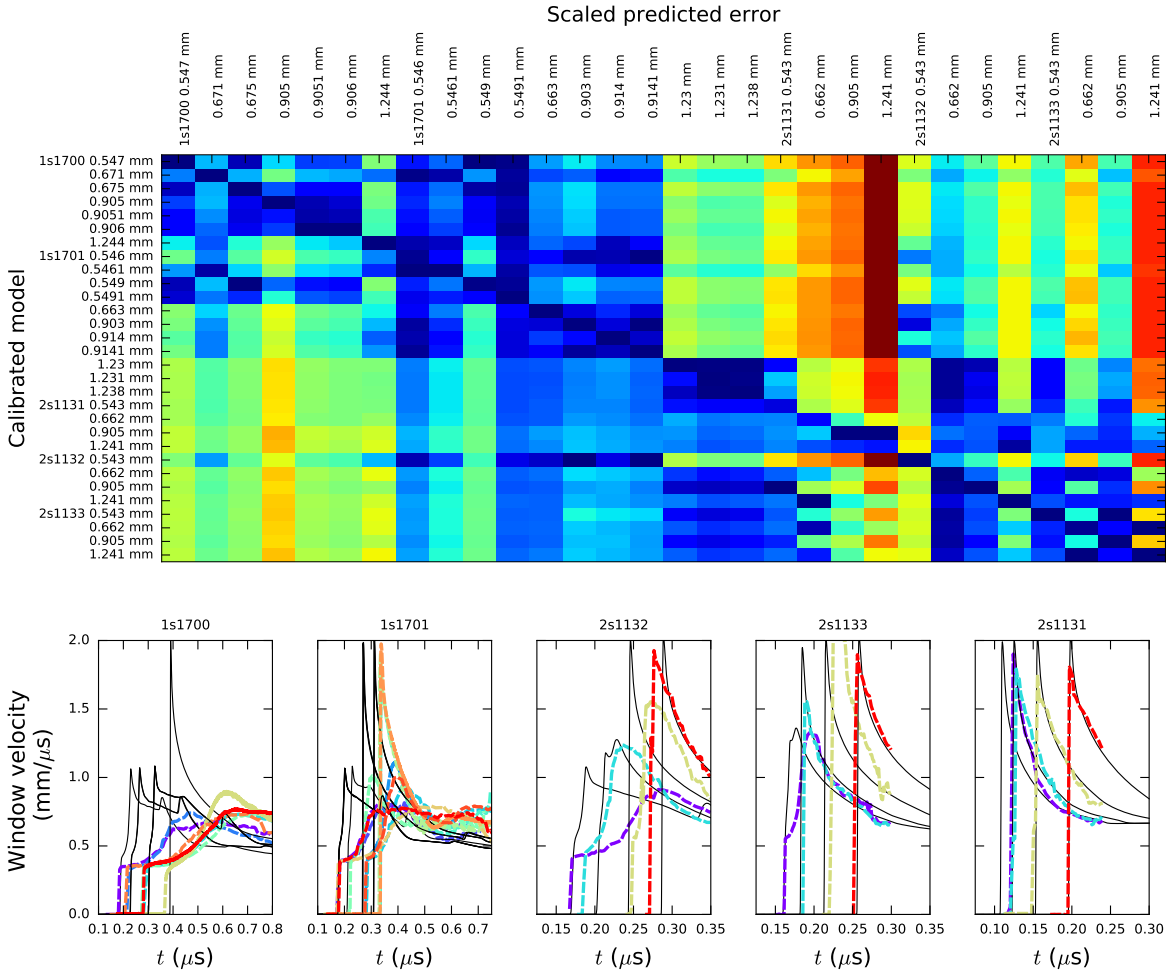

Figure 4: (top) An error matrix plot correlating individual calibrations of a single window profile and their associated prediction of corresponding window profiles for all other experimental conditions. (bottom) The calculated (solid black lines) and window velocity measurements (colored dashed lines).

relatively poor in predicting the more reactive profiles. This observation may point to a generic effect of extrapolating sufficiently incomplete reactive profiles to detonation but requires more investigation.

As a result of the disjoint behavior which makes a single parameterization with uniform fit error difficult to obtain, our initial modeling effort was restricted to the *higher pressure regime* which also more relevant to our intended application. The results of the high pressure data calibration process are shown in Fig. 4(bottom). Parameters for the initiation rate term appear in Table 2. The correspondence is naturally far better for the higher input pressure shots as the 1s-1700 and 1s-1701 shots are not included in the calibration source data. The model-calculated Pop-plot trend line also appears in Fig. 2, showing an intermediate sensitivity relative to the experimental trend lines [2] for lower (1.6 g/cm^3) and higher pressing densities (1.72 g/cm^3), as expected.

4 Conclusions

Our new experimental results provide a necessary and significant expansion of reactive build-up data for the extremely ideal PETN explosive. Further experiments are underway to confirm the pronounced

Table 2: Calibrated parameters of the modified WSD model.

Davis reactants			Davis products			Reaction rate		
						Initiation		
$A =$	1.4040	mm/μs	$a =$	0.5675		$k_i =$	0.0060672	μs^{-1} GPa^{-y}
$B =$	2.0035		$b =$	0.6752		$y =$	3.93323	
$C =$	10.6064		$n =$	1.4276		$\rho_c =$	2.75	g/cm^3
$\alpha =$	0.3309		$k =$	1.3110				
$\Gamma_{r,0} =$	0.7148		$v_c =$	0.6707	cm^3/g		Propagation	
$Z =$	0.0		$p_c =$	9.9887	GPa	$k_g =$	0.0088988	μs^{-1} GPa^{-n}
$\rho_0 =$	1.65	g/cm^3	$E_{det} =$	6.856	kJ/g	$n =$	3.5	
$T_0 =$	297	K				$c =$	0.8	

difference in sensitivity depending on the input pressure, a trend quantified via reactive flow model calibration analysis. If confirmed, these forthcoming experiments will be essential in guiding further model development efforts. A subset of this data was used to complete a reactive burn model for the explosive which also directly incorporates the recently available metal acceleration and timing data [4].

References

[1] G. E. Seay and L. B. Seely. Initiation of a low-density PETN pressing by a plane shock wave. *J. Appl. Phys.*, 32(6):1092–1097, 1961.

[2] D. Stirpe, J. O. Johnson, and J. Wackerle. Shock initiation of XTX-8003 and pressed PETN. *J. Appl. Phys.*, 41(9):3884–3893, 1970.

[3] P. C. Souers and J. W. Kury. Comparison of cylinder data and code calculations for homogeneous explosives. *Prop. Expl. Pyro.*, 18(4):175–183, 1993.

[4] E. K. Anderson, C. Chiquete, R. I. Chicas, and S. I. Jackson. Detonation performance experiments, modeling, and scaling analysis for pentaerythritol tetranitrate (PETN) high explosive. *Prop. Expl. Pyro.*, 47(9):e202200069, 2022.

[5] T. D. Aslam, C. A. Bolme, K. J. Ramos, M. J. Cawkwell, C. Ticknor, M. A. Price, J. A. Leiding, N. J. Sanchez, and S. A. Andrews. Shock to detonation transition of pentaerythritol tetranitrate (PETN) initially pressed to 1.65 g/cm^3. *J. Appl. Phys.*, 130(2):025901, 2021.

[6] B. L. Wescott, D. S. Stewart, and W. C. Davis. Equation of state and reaction rate for condensed-phase explosives. *J. Appl. Phys.*, 98:053514, 2005.

[7] E. K. Anderson, C. Chiquete, S. I. Jackson, R. I. Chicas, and M. Short. The comparative effect of HMX content on the detonation performance characterization of PBX 9012 and PBX 9501 high explosives. *Combust. Flame*, 230:111415, 2021.

[8] C. Chiquete, S. I. Jackson, E. K. Anderson, and M. Short. Detonation performance experiments and modeling for the DAAF-based high explosive PBX 9701. *Combust. Flame*, 223:382–397, 2021.

[9] C. Chiquete and S. I. Jackson. Detonation performance of the CL-20-based explosive LX-19. *Proc. Combust. Instit.*, 38(3):3661–3669, 2020. doi: https://doi.org/10.1016/j.proci.2020.07.089.

[10] C. Chiquete, M. Short, C. D. Meyer, and J. J. Quirk. Calibration of the pseudo-reaction-zone model for detonation wave propagation. *Combust. Theory Modell.*, pages 744–776, 2018.

[11] J. J. Quirk. amr_sol::multimat. Technical Report LA-UR-07-0539, Los Alamos National Laboratory, U.S.A., 2007.